NMR IN BIOMEDICINE
NMR Biomed. 1999;**12**:157–167

Differences in metabolism of 5-fluorouracil and 5-fluorouridine and regulation by glucosamine in human colon cancer multicell tumor spheroids

Tong-Bin Chen,[1] Željko Bajzer,[2] Slobodan Macura[2] and Stanimir Vuk-Pavlović[1,2]*

[1]Division of Developmental Oncology Research, Department of Oncology, Mayo Clinic and Mayo Foundation, Rochester, MN 55905, USA
[2]Department of Biochemistry and Molecular Biology, Mayo Clinic and Mayo Foundation, Rochester, MN 55905, USA

Received 8 December 1997; revised 17 April 1998; accepted 27 April 1998

ABSTRACT: Glucosamine (GlcN) modulates fluoropyrimidine metabolism and enhances cytotoxicity of 5-fluorouridine (FUrd), but not of 5-fluorouracil (FUra), in human tumor models. To elucidate the underlying metabolic differences between FUra and FUrd, by the use of ^{19}F and ^{31}P NMR spectroscopy we studied these drugs in multicell tumor spheroids (MTS) formed by human colon carcinoma cells HT-29. This experimental system allowed detailed kinetic measurements of anabolic intracellular phosphates and fluorophosphates over periods of up to 2 days. Time-dependent NMR data were reduced and interpreted by the use of nonlinear compartmental models which yielded numerical values for the empirical rate constants characterizing mass transfer among the compartments. An analysis of these rate constants indicated qualitative and quantitative differences in the metabolism of FUra and FUrd and in the effects of GlcN on these drugs. The enhanced generation of FUDP-hexoses was a predicted effect of GlcN, but inhibited formation of fluorouridine diphosphates and fluorouridine triphosphates in FUra-treated MTS, and the magnitude of stimulation of fluoropyrimidine incorporation into macromolecules in FUrd-treated MTS were not predicted. Copyright © 1999 John Wiley & Sons, Ltd.

INTRODUCTION

Forty years ago FUra was suggested as an anticancer drug,[1] yet the precise molecular mechanism of its action is still unclear.[2] The rationale for the continuing search for this mechanism has been not only the need to understand how the widely used FUra works, but also the hope that a better understanding of the mechanism will make it possible to increase the efficacy and tumor specificity of this drug by modulation with other pharmacological agents.[2–4] The latter view stimulated the quest for biochemically defined 'critical' intracellular targets that are inhibited by a FUra metabolite leading to a predictable cellular response. A critical target has not yet been identified *in vivo*, leaving open the possibility that cell death results from interference of the drug with numerous intracellular processes.[5]

The view that the cytotoxic action of FUra is determined by factors beside intracellular concentration of the drug and its metabolites has been supported by experiments. For example, after exposure to FUra, cells replated as monolayers were markedly more sensitive to the cytotoxic effect of FUra than cells maintained in three-dimensional collagen clusters.[6,7] Human colon carcinoma cells HT-29 grown as multilayers were 40 times more resistant to FUra than the cells grown as monolayers,[8] in line with the general observation that cells in multicell assemblies are more resistant to drugs than when grown as monolayers (cf. Frankel *et al.*[9] and references therein). Thus, *in vitro* data might be more relevant to the understanding of FUra pharmacology when obtained in three-dimensional cellular assemblies.

Recently, we employed ^{19}F magnetic resonance spectroscopy to study interactions of FUra and FUrd with octreotide, a long-acting somatostatin analogue, in multicell tumor spheroids (MTS) comprised of human colon carcinoma cells designated HT-29.[10] We found that the metabolism of FUra was kinetically different and differently regulated by octreotide from the metabolism of FUrd. However, molecular details of octreotide effects on fluoropyrimidine metabolism are unknown and, in the absence of a documented model of FUra metabolism in

**Correspondence to:* S. Vuk-Pavlović, Guggenheim 1311A, Mayo Clinic, Rochester, MN 55905, USA.
E-mail: vuk_pavlovic@mayo.edu
Contract/grant sponsor: Fraternal Order of Eagles.

Abbreviations used: AzaUrd, 6-azauridine; FdUMP, 5-fluoro-2′-deoxyuridine-5′-monophosphate; FUDP, 5-fluorouridine-5′-diphosphate; FUDP-Hex, 5-fluorouridine-5′-diphosphate-*N*-acetyl-hexosamines; (F)UDP-Hex, UDP-Hex plus FUDP-Hex; FUra, 5-fluorouracil; FUrd, 5-fluorouridine; FUTP, 5-fluorouridine-5′-triphosphate; GlcN, glucosamine; MTS, multicell tumor spheroids; NDPs, nucleotide diphosphates; NTPs, nucleotide triphosphates; ppm, parts per million; UDP-Hex, uridine-5-diphosphate hexoses.

CCC 0952–3480/99/030157–11 $17.50

MTS, we could only speculate on a mechanistic interpretation of these effects.

In our efforts to develop a model of regulation of fluoropyrimidine metabolism in MTS, here we studied glucosamine effects on FUra and FUrd metabolism in MTS monitored by ^{19}F and ^{31}P magnetic resonance spectroscopy.[5,11–13] We selected the interaction of fluoropyrimidines and glucosamine in HT-29 cells because this experimental system has been characterized rather well,[14] and it thus provides a good empirical basis for our studies. GlcN is particularly well suited for these studies because it introduces major and measurable perturbations into fluoropyrimidine metabolism in MTS without apparent toxicity in HT-29[14] and other cells[15] during experiments. We obtained rather detailed information on the kinetics of development of intracellular fluoropyrimidine anabolites and analyzed these data by a nonlinear compartmental model of fluoropyrimidine metabolism. We found that GlcN reduced the generation of FUDP/FUTP in FUra-treated MTS, and had no effect on the incorporation of FUra into macromolecules. On the other hand, in FUrd-treated MTS, GlcN did not limit the generation of FUDP/FUTP, but strongly stimulated fluoropyrimidine incorporation into macromolecules.

MATERIALS AND METHODS

NMR spectra of spheroid suspensions

MTS comprising human colon adenocarcinoma cells HT-29 were initiated and maintained as described before.[10] A 1.0 ml amount of settled spheroids was perfused in the NMR tube (10 mm diameter) by an apparatus that maintained a steady flow of 2.0 1 thermostatted (sample temperature 37°C) sterile serum-free tissue culture medium with controlled pH and oxygen consumption.[10] NMR spectra were obtained with a Bruker AMX-300 spectrometer. ^{31}P signals were accumulated at 121.50 MHz, with 60° pulses, 558 scans per spectrum, 0.45 s acquisition time (AQ) and 6 s relaxation delay. Under these conditions, we determined that the resonances under study were not saturated. Spectra were recorded every 60 min and processed with a resolution enhancement filter, Lorentz to Gauss transform, $\exp[-\pi \times LB \times t + \pi \times LB \times t^2 / (2 \times GB \times AQ)]$, with $LB = -10$, $GB = 0.0215$ and $AQ = 0.45$.

To determine the relative amounts of phosphorus-containing species in MTS, NMR spectral peaks were resolved by our own interactive computer program (written in MLAB, Civilized Software, Bethesda, MD), which included the following algorithm: (1) preliminary baseline adjustment by fitting the experimental baseline on both sides of the spectrum to a straight line; (2) visual peak identification with preliminary positioning of maximum height; (3) preliminary determination of peak width at half-maximum height by approximating the peak shape with an isosceles triangle; the base of the triangle was defined by the *x*-axis of the spectrum, the altitude by the point of maximum peak height, and the side by a line fitted through the maximum and several adjacent points of the digitized spectrum which define the upper ascending or descending half of the peak; (4) repeating steps 1–3 for each peak in the spectrum; this procedure yielded the initial guesses for the values of position, width and height of individual Gaussian shaped peaks; (5) fitting the sum of Gaussian functions and the base line to data; and (6) quantifying the peak area by integration under each deconvoluted peak.

^{19}F spectra were measured at 282.36 MHz, with 60° pulses, 1000 scans per spectrum, 160 ms acquisition time and 4 s relaxation delay. Longer relaxation delays did not change the intensity of the observed resonances, consistent with fully relaxed NMR spectra. ^{19}F spectra were recorded every 70 min. Areas under the curves in the spectra, determined as above, were used as relative amounts and were compared with the known concentrations of FUra or FUrd in the medium at the beginning of experiment.

All experiments were done at least in duplicate with qualitatively analogous results. Examples are presented which yielded statistically better best-fit parameter estimates.

Assignment of ^{19}F spectra and origins of ^{19}F signals

The ^{19}F resonances were assigned previously in the spectra, recorded at 22°C, of perchloric acid extracts of MTS treated with FUra for 30 h.[10] The ^{19}F spectrum showed five distinct peaks: FUra (for convenience, arbitrarily assigned at 0.00 ppm), FUMP (5.09 ppm), FUDP (4.61 ppm), FUTP (4.71 ppm) and FUDP-Hex (4.99 ppm). The FUDP-Hex peak includes FUDP-sugars with resonances within the range of 0.04 ppm.[16] In the spectra of extracts of MTS treated with FUra for 10 and 20 h, respectively, the height of the FUMP peak was less then half the height at 30 h (not shown). On the basis of these data, resonances in intact MTS were assigned as FUDP/FUTP (4.90 ppm) and FUMP/FUDP–Hex (5.04 ppm). No other signals were detected within the range of 44.27 ppm upfield and downfield relative to FUra, including the FdUMP resonance 0.23 ppm downfield from FUMP.[17] The FUrd resonance was centered at 3.83 ppm relative to FUra.[10]

After experiments, cell-free perfusates gave rise only to ^{19}F resonances originating from FUra or FUrd, indicating that signals from metabolites originated entirely from MTS.[10] Also, in intact MTS washed free of FUra or FUrd in the medium, the resonances at 0.00 or 3.83 ppm were not detectable, indicating that intracellular FUra and FUrd were not detectable by NMR, probably due to immobilization by adsorption to macromolecules.

In MTS treated with either FUra or FUrd, the resonance at 4.90 ppm (FUDP/FUTP) appeared before the resonance at 5.04 ppm (FUMP and FUDP-Hex; Fig. 4a, b). FUMP is the obligatory precursor of FUDP and FUTP, but in extracts its amounts were small relative to the amounts of FUDP-Hex. Also, in MTS with *de novo* synthesis of UMP inhibited by AzaUrd (Fig. 6e, f), introduction of FUrd gave rise to the ^{19}F resonance at 5.04 ppm (Fig. 6f); this rise was paralleled by a similar rise in the ^{31}P resonances attributed solely to FUDP-Hex (Fig. 6e). Consequently, it appears that the amounts of FUMP in intact MTS were below detection and, thus, the resonance at 5.04 ppm was due mostly to FUDP-Hex.

Compartmental analysis of NMR data

For data reduction, we designed a compartmental model of fluoropyrimidine mass transfer. We modeled the kinetics of mass transfer among the *observed* compartments, rather than on the multitude of unobservable elemetary chemical steps. The advantage of the mass transfer model is in the ability to estimate the four empirical rate constants with statistical soundness; the estimation of at least twice as many true kinetic rate constants from the same data would not withstand statistical scrutiny.

The model is compatible with FUra and FUrd metabolism[15] and accounts explicitly for data measured in MTS by ^{19}F-NMR (Fig. 1):

$$\begin{aligned} dF_p(t)/dt &= kF_0(t-\tau) + k_f F_g(t) \\ &\quad - k_r F_p(t) \\ &\quad - k_g F_p(t)\ G(t); \qquad F_p(0) = 0 \end{aligned} \tag{1}$$

$$dF_g(t)/dt = k_g F_p(t)\ G(t) - k_f F_g(t); \quad F_g(0) = 0 \tag{2}$$

$$dG(t)/dt = -k_g F_p(t)\ G(t); \qquad G(0) = g > 0 \tag{3}$$

F_0(t) in eq. 1 represents the FUra or FUrd concentration in the medium; for mathematical convenience, and to account for the asymptotic behavior of F_0, we modeled the time dependence of F_0 as the simple exponential decay:

$$F_0 = f\,e^{-\lambda t} \quad F_0(0) = f > 0 \tag{4}$$

consistent with observations of almost linear decrease of F_0 with time (see Figs 5 and 6). The phenomenological constant λ accounts for depletion of FUra or FUrd from the medium due to uptake by MTS. The rate of concentration change in F_p (FUDP/FUTP), due to transport of FUra or FUrd and their subsequent phosphorylation, is modeled by the input function $k\,F_0(t-\tau)$ where the rate constant k characterizes the rate of transmembrane transport and the time delay τ accounts for the kinetic influence of the NMR-undetectable intracellular FUra or FUrd.

By the use of the specific form, eq. 4, of F_0, eq. 1 can be expressed as:

$$dF_p(t)/dt = k_p F_0(t) + k_f F_g(t) - k_r F_p(t) - k_g F_p(t)\ G(t) \tag{5}$$

where

$$k_p = k e^{\lambda\tau} \tag{6}$$

is the effective rate constant characterizing input to the F_p compartment. Thus, our kinetic model does *not* deal with (undetectable) intracellular FUra and FUrd explicitly and does *not* model different mechanisms of their transmembrane transport, but it accounts for these phenomena implicitly, as reflected in best-fit values of the constant k_p.

We modeled the buildup of F_g as a second-order process (rate constant k_g) that depends both on F_p and G (extracellular glucose and GlcN; eqs 1 and 2; cf. Holstege *et al.*[15]). On the other hand, catabolism of F_g is modeled as first-order decay (rate constant k_f) dependent on the rate of generation of FUDP from FUDP-Hex.[2] In this

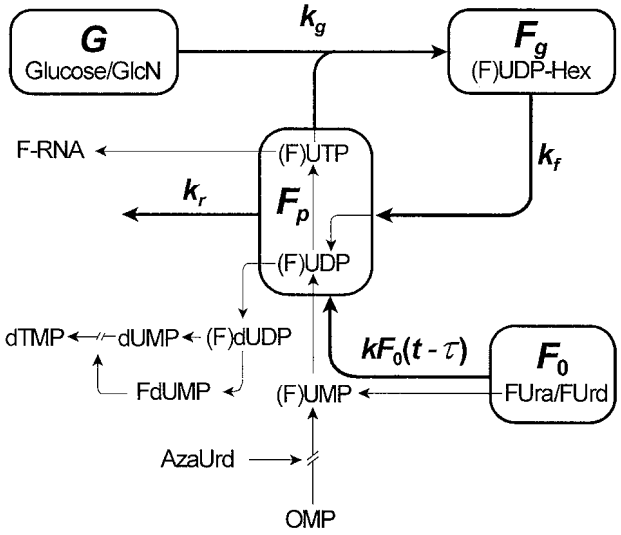

Figure 1. Compartmental model of fluoropyrimidine transfer in multicell tumor spheroids [bold; eqs 1–4 in the text] laid over the schematic of pertinent aspects of fluoropyrimidine metabolism (fine lines; adapted from Holstege and Kepler[5]). In cells, FUra and FUrd are converted into FUDP and FUTP (via FUMP) further giving rise to FdUMP, F-RNA and FUDP-Hex. The mass transfer model accounts explicitly for NMR detectable compartments only. F_0 stands for the concentration of FUra or FUrd in the medium, diminished at a rate characterized by the term $kF_0(t-\tau)$. The symbol F_p denotes intracellullar FUDP and FUTP created by the process characterized by the rate constant k and k_f. F_g stands for FUDP-Hex, and G for glucose and GlcN in the medium (in the same physical volume as F_0). Buildup of F_g was modeled as a second-order rate process (rate constant k_g) and degradation as first-order decay (k_f). The constant k_r represents the rate of loss of fluoropyrimidine phosphates from F_p into species undetectable under our experimental conditions (F-RNA, FdUMP, FdUDP; for explanation, see text). Breaks in arrows indicate the site of inhibition of deoxythymidine monophosphate (dTMP) formation by FdUMP and of UMP formation (from orotidine monophosphate, OMP) by AzaUrd

model, glucose and glucosamine are lumped into the same compartment G because the two molecules are routed into the same metabolic pathway via glucosamine-6-phosphate (cf. Pederson *et al.*[18]). Finally, the rate constant k_r characterizes the 'loss' of ^{19}F signal to the incorporation of fluorinated metabolites into macromolecules (e.g. F-mRNA). The symbols 'f' and 'g' in eqs 4 and 3, respectively, stand for initial concentrations of FUra or FUrd and glucose without or with glucosamine in the medium, respectively.

The model functions were fitted to time-dependent relative concentrations (obtained as integrals under spectral peaks) corresponding to compartments F_0, F_p and F_g taking into account the known initial value of $G(0) = g$.

For a reliable estimation of rate constants λ, k_p, k_f, k_g and k_r, we designed and used the following three-step procedure:

Step 1. Parameters f and k were determined by fitting the function $F_0(t) = fe^{-\lambda t}$ [eq. 4] to data using the least-squares method. The initial guesses for f and λ were obtained by solving the equations $\ln \mathcal{F}_0(t_j) = \ln f - t_j$, $j = 1, 2$, where $\mathcal{F}_0(t_j)$ are measured concentrations of FUra (or FUrd) in the medium at times t_j.

Step 2. Equation 4 and the sum of eqs 5 and 2 were integrated formally from 0 to t_i, yielding

$$F_g(t_i) + F_p(t_i) = k_p[f - F_0(t_i)]/\lambda - k_r \int_0^{t_i} F_p(t)dt = \psi_i(k_p, k_r) \quad (7)$$

where t_i, $i = 1, \ldots, n$ are data sampling times for F_0, F_g and F_p. In the spirit of the least-squares method, the function

$$\sum_1^n [\mathcal{F}_g(t_i) + \mathcal{F}_p(t_i) - \psi_i(k_p, k_r)]^2 \quad (8)$$

was minimized with respect to k_p and k_r. Here $\mathcal{F}_g(t_i)$ and $\mathcal{F}_p(t_i)$ denote measured metabolite concentrations at times t_i; the integral in eq. 7 was estimated by the use of $\mathcal{F}_p(t_i)$ and the trapezoidal rule. The parameters f and λ and thus $F_0(t_i)$ were determined in Step 1. Note that eq. 8 could be minimized analytically because the term $\psi_i(k_p, k_r)$ is linear in variables (linear least-squares method); consequently, the initial guess values for k_p and k_r were not needed.

Step 3. The estimates of k_p and k_r were now used as initial guesses for the global fitting of $\mathcal{F}_p(t_i)$ and $\mathcal{F}_g(t_i)$ with respect to k_p, k_r, k_f and k_g, i.e. the χ^2-function

$$\chi^2 = S(k_p, k_r, k_f, k_g) = \sum_1^n [\mathcal{F}_p(t_i) - F_p(t_i)]^2 + [\mathcal{F}_g(t_i) - F_g(t_i)]^2 \quad (9)$$

was minimized. Here $F_p(t_i)$ and $F_g(t_i)$ were determined by numerical solution of eqs. 1–3. The computer code was written in MLAB;[19] this programming platform contains a user-friendly least-squares fitting procedure for functions defined by differential equations. Also, this fitting procedure yielded the local Hessian from which errors in parameters were estimated.

Statistical analysis

By the use of the above procedure, we evaluated different models for each data set, i.e. we fitted the model functions with k_r and/or k_f set to zero. The significance of differences among χ^2-values for best fits by the models were assessed by the F-test,[20] and the chosen model parameters and best-fit curves are shown in Table 1 and Figs 5 and 6, respectively.

The significance of differences among best-fit parameters (i.e. kinetic constants describing a process under different experimental conditions; data in Figs 5 and 6) was assessed by the probability p that the difference between the estimated parameter values was zero. We assumed a Gaussian distribution of kinetic parameters with means and their standard deviations obtained by least-squares fitting of eqs. 1–4 to data. The statistic z for the two-tail hypothesis test was[21] $z = (k_a - k_b)/(\sigma_a^2 + \sigma_b^2)^{1/2}$, where k_a and k_b are best-fit values of the rate constants for experimental conditions a and b with σ_a and σ_b as the corresponding standard deviations.[21] When $p < 0.01$, we considered the values of the respective best-fit parameters statistically different.

The significance of differences among the time-dependent concentration changes in Fig. 3 was assessed by fitting straight lines through data points and analyzing, by the procedure described above, the significance of differences between the respective regression slopes.

RESULTS

^{31}P NMR measurements of phosphate metabolism in MTS

To characterize the kinetics of changes in metabolism of intracellular phosphates induced by GlcN and AzaUrd, we recorded ^{31}P NMR spectra in MTS suspensions as a function of time. The ^{31}P NMR spectrum of HT-29 cell MTS in the serum-free high-glucose McCoy's 5A medium (3 mg/ml; Fig. 2a) demonstrated the typical intracellular NMR-detectable phosphates and the high levels, characteristic of these cells, of intracellular diphosphodiesters (UDP-Hex) with the multiple overlapping α-phosphate peaks centered around -8.3 ppm and the β-phosphate peaks around -10 ppm relative to phosphocreatine (arbitrarily set to 0 ppm), respectively (see the front spectrum in Fig. 2; cf. Sheed *et al.*[22]). The contribution of NAD(H) resonances to the peak at -8.3 ppm was not determined, but was not significant;[22]

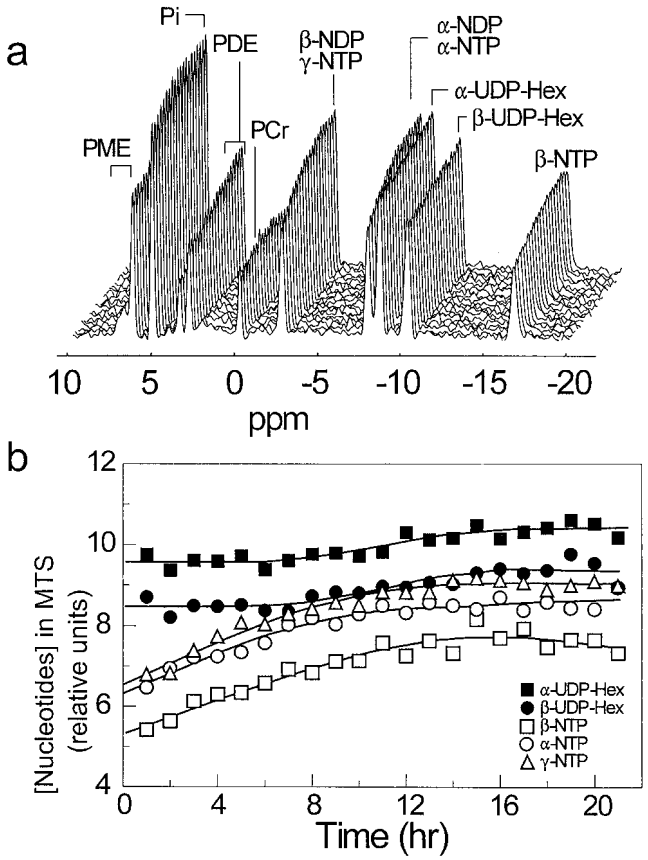

Figure 2. (a) ^{31}P NMR spectra of HT-29 multicell tumor spheroids perfused in serum-free McCoy's 5A medium with FUrd (0.19 mM) at 37°C obtained with a Bruker AMX-300 spectrometer at 121.50 MHz, 30 μs pulse width, 558 scans per spectrum, 6 s repetition time and 0.45 s relaxation delay. Accumulations for each spectrum were initiated every 60 min. The origin of the scale is set at the maximum of the phosphocreatine (PCr) peak. PME, phosphomonoesters; Pi, inorganic phosphate; PDE, phosphodiesters; NDP, nucleotide diphosphates; NTP nucleotide triphosphates; UDP-Hex, uridinediphosphate hexoses. (b) Data from (a) shown as relative concentrations (areas under peaks) for α-UDP-Hex, β-UDP-Hex, α-NTPs, β-NTPs and γ-NTPs

this conclusion is corroborated by the observation that the changes in peaks assigned to α-phosphate and to β-phosphate were always equivalent and parallel (cf. Figs 2b and 3), i.e. the changes in α-resonances and β-resonances were affected by the same mechanism.

To determine the extent of changes in intracellular phosphates in HT-29 cell MTS perfused in the NMR tube for 24 h (the average duration of experiments), we recorded ^{31}P NMR spectra every hour for 24 h and plotted the integrals under peaks, proportional to relative concentrations of the respective chemical species, as a function of time (Fig. 3a). Figure 3a shows the increase in relative concentrations of α-, β- and γ-phosphates in NTPs and NDPs and the rather steady α- and β-phosphates in UDP-Hex. The apparent changes in the levels of intracellular NDPs and NTPs were compatible with the changes in cellularity of MTS in the NMR tube; after 24 h in the absence of drugs, the volume of settled spheroids increased by about 10% relative to the volume at the beginning of experiment (data not shown). In all experiments, the quantitative changes in β-NTP resonances were roughly equivalent to the changes in α-NDP/α-NTP and β-NDP/γ-NTP phosphates, indicating that the majority of observed effects were changes in concentrations of NTPs.

Introduction of GlcN (10 mM) at the beginning of ^{31}P NMR spectra accumulation induced significant changes in the distribution of intracellular phosphates (Fig. 3b). Concentrations of UDP-Hex increased continuously, while NTPs remained almost unchanged. Relative to controls (Fig. 3a), the presence of GlcN increased the UDP-Hex concentrations by one half ($p < 0.01$ for the difference in slopes of concentration change). At the same time, the NTP concentrations in Fig. 3b remained steady, while those in control MTS increased by one third ($p < 0.01$ for the difference in slopes of concentration change). This observation is consistent with GlcN-stimulated formation of UDP-Hex which results in depletion of UTP.[14,15]

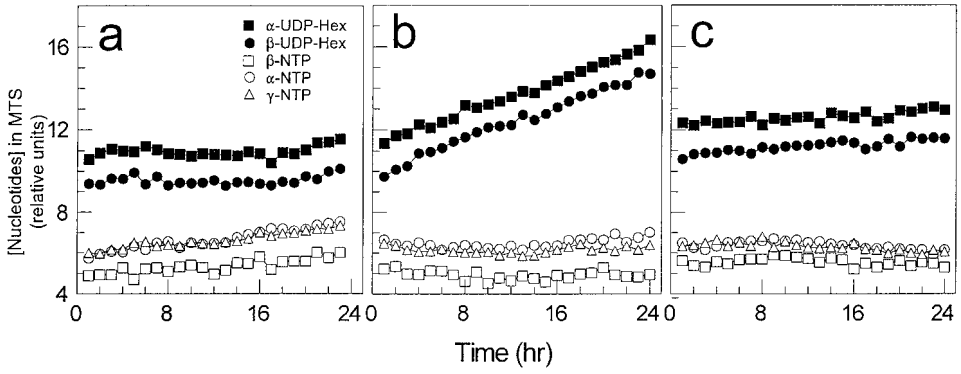

Figure 3. (a) Relative concentrations (areas under peaks) for α-UDP-Hex, β-UDP-Hex, α-NTPs, β-NTPs, and γ-NTPs in MTS perfused in serum-free McCoy's medium for 24 h; (b) same as (a) for MTS perfused in 10 mM GlcN; (c) same as (a) for MTS perfused with AzaUrd (0.5 mM) and GlcN (10 mM)

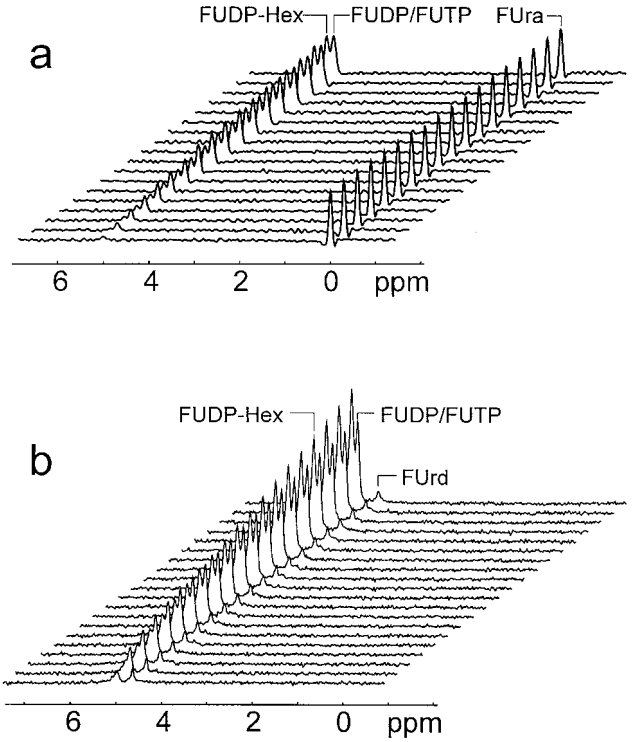

Figure 4. (a) ^{19}F spectra of MTS incubated in FUra (initial concentration, 0.77 mM) measured at 282.36 MHz, 40 μs pulse width, 1000 scans per spectrum, 4 s repetition time and 160 ms acquisition time. ^{19}F spectra were recorded every 70 min. (b) Same as (a), except that MTS were incubated with FUrd (initial concentration, 0.19 mM). FUDP-Hex, fluorouridine diphosphate hexoses; FUDP/FUTP, fluorouridine diphosphate and fluorouridine triphosphate

To demonstrate that the relative decrease in NTPs was indeed coupled with enhanced UDP-Hex formation,[14,15] we inhibited *de novo* pyrimidine synthesis by AzaUrd (0.5 mM) in the presence of GlcN (10 mM) and recorded ^{31}P NMR spectra as before. As expected, AzaUrd inhibited GlcN-stimulated UDP-Hex formation (Fig. 3c; $p < 0.01$ for the difference of slopes in Fig. 3b and c), compatible with depletion of NTPs by GlcN in Fig. 3b being caused by the metabolic conversion of UTP into UDP-Hex. Interestingly, the relative contribution of NTPs (as measured by β-NTP) increased in these cells, as indicated by the diminished difference between the β-NTP resonances on one hand and the α-phosphate and the β-NDP/γ-NTP resonances on the other.

Modulation of fluoropyrimidine metabolism by GlcN

To determine the effects of FUra and FUrd on phosphate metabolism and cell viability under our experimental conditions, we recorded ^{31}P spectra of MTS incubated with FUra (0.77 mM) or FUrd (0.19 mM) over 22–24 h. A typical set of spectra is shown in Fig. 2; the experiment was initiated by the introduction of FUrd to MTS. An examination of these spectra reveals that the maxima representing (F)UDP-Hex remained rather constant, while NTPs increased steadily. The plot of relative concentrations of (F)UDP-Hex and NTPs derived from maxima in Fig. 2 as a function of time showed that (F)UDP-Hex increased with time linearly, similarly to that in MTS without fluoropyrimidines (Fig. 3a). The amounts of NTPs, however, increased more strongly for the first 12 h and then reached a plateau at a level similar to the amount of (F)UDP-Hex (see also Fig. 6a). This observation indicates continued metabolism and cell viability throughout the experiment.

Changes in intracellular levels of fluorophosphates in MTS induced by FUra (0.77 mM) in the medium are shown as time-dependent stacked ^{19}F spectra in Fig. 4a, as time-dependent relative concentrations of phosphates (measured by ^{31}P NMR) in Fig. 5a and of fluorophosphates (measured by ^{19}F NMR) in Fig. 5b, respectively.† ^{31}P NMR data were obtained within the first, 24th and 48th hour of experiment (Fig. 5a). FUra was introduced into the medium at the beginning of the 25th hour and successive ^{19}F spectra were each obtained by a 70-min signal accumulation (Fig. 5b).

Concentrations of extracellular FUra decreased steadily with time, while the amounts of intracellular FUDP/FUTP and FUDP-Hex steadily increased (Fig. 5b). Simultaneously, the increase in amounts of intracellular (F)UDP-Hex and (F)NTPs in the presence of FUra (25–48 h; Fig. 5a) was consistent with the changes in ^{19}F spectra. These changes in the levels of (F)UDP-Hex and (F)NTPs detected by ^{31}P NMR (25–48 h) have probably resulted only from the treatment with FUra, because such a relative increase in UDP-Hex and NTPs was not detectable in control MTS (data not shown).

To determine the effect of depletion of intracellular NTP pools (i.e. predominantly UTP) on FUra uptake and metabolism,[14] we introduced FUra into MTS pretreated for 24 h with GlcN (10 mM). This and further treatment with GlcN reduced the amounts of intracellular FUDP/FUTP and FUDP-Hex (Fig. 5d) relative to MTS not treated with GlcN (Fig. 5b). Also, (pre)treatment with GlcN reversed the magnitudes of concentrations of FUDP/FUTP vs FUDP-Hex (Fig. 5b and d), i.e. in the presence of GlcN, the levels of FUDP/FUTP were much lower than of FUDP-Hex; the reversal of levels in FUDP/FUTP and FUDP-Hex indicates that the conversion of FUDP/FUTP into FUDP-Hex was relatively more efficient in GlcN-treated spheroids. GlcN reduced the levels of NTPs and increased the levels of UDP-Hex in the absence of FUra (Fig. 5c). The presence of FUra increased the levels of NTPs.

†Note that in Fig. 2 of Chen *et al.*,[10] the squares were mistakenly described as FUDP-Hex and triangles as FUTP/FUDP; the opposite is correct, i.e. the symbols in Chen *et al.*[10] mean the same as in Figs 5b, 5d, 6b, 6d and 6f in this paper, respectively.

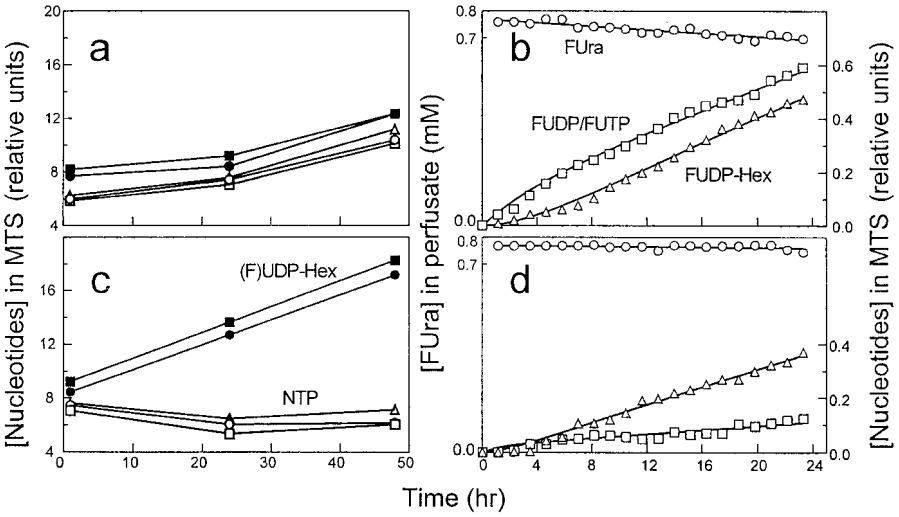

Figure 5. (a) and (c) Time dependence of intracellular levels of (fluoropyrimidine)phosphates measured by ^{31}P NMR in MTS perfused with serum-free McCoy's 5A medium in the absence (a) and presence of 10 mM GlcN (c) measured as in Fig. 2 during the 1st, 24th and 48th hour of the experiment. Symbols as in Fig. 2b. FUra (initial concentration, 0.77 mM) was added to MTS at the beginning of the 25th hour. (b) and (d) Time dependence of FUra concentrations in perfusates and of the amounts of metabolites in MTS with McCoy's 5A medium was measured by ^{19}F NMR without (b) and with 10 mM GlcN (d); same samples as in (a) and (c), respectively. Data points represent magnitudes of integrals under spectral peaks obtained in MTS incubated with FUra. Zero time in (b) and (d) corresponds to the 25th hour (addition of FUra) in (a) and (c). The lines are best-fit curves obtained by fitting the functions of the compartmental model described by eqs 1–4 to data

Experiments such as those in Fig. 5 were performed also with FUrd (0.19 mM; Figs 3b and 6). Introduction of FUrd increased the NTP levels relative to UDP-Hex as detected by ^{31}P NMR (Fig. 6a; see also Fig. 2b). ^{19}F NMR spectra revealed that FUrd, positioned at 3.83 ppm relative to FUra, was taken up and metabolically converted by MTS (Fig. 6b) more efficiently than FUra (Fig. 5b). The amount of FUDP/FUTP rapidly increased up to 300 min and then slowed down and became more linear. Simultaneously, the amounts of FUDP-Hex increased linearly beyond the levels reached in MTS treated with FUra (Fig. 5b). Interestingly, increases in FUDP/FUTP observed in Figs 5b and 6b were paralleled by similar increases in NTPs upon addition of FUra and FUrd, respectively (Figs 5a and 6a). This time dependence is consistent with the similar time dependence of NTPs in Fig. 2b and FUDP/FUTP in Fig. 6b—both reached a plateau in 12 h.

Introduction of FUrd to MTS (pre)treated with GlcN resulted in low levels of intracellular FUDP/FUTP (Fig. 6d) compared with MTS in Fig. 6b. At the same time, the levels of FUDP-Hex rose steadily, albeit somewhat more slowly than in Fig. 6b. The control ^{31}P NMR spectra revealed that the NTP levels in these MTS remained unchanged by the addition of FUrd, while the levels of FUDP-Hex increased (Fig. 6c).

To assess the role of UTP replacement by *de novo* synthesis in GlcN-treated MTS, we inhibited UMP formation by AzaUrd (0.5 mM). This treatment did not change the levels of NTPs and UDP-Hex in MTS, but introduction of FUrd sharply elevated the levels of (F)UDP-Hex (Fig. 6e). The ^{19}F spectra revealed a similar absence of a major change in the levels of FUDP/FUTP, but the levels of FUDP-Hex (Fig. 6f) increased beyond the levels reached by MTS with uninhibited UMP formation (Fig. 6b and d).

The comparison of data in Figs 5 and 6 indicated that the buildup of FUDP/FUTP proceeded faster in MTS treated with FUrd relative to MTS treated with FUra. Incubation with GlcN reduced the levels of FUDP/FUTP in MTS treated with either drug, but in FUrd-treated spheroids the levels of FUDP/FUTP were maintained at a steady state that was established 4 h following FUrd introduction. Interestingly, the large differences in FUDP/FUTP buildup between control MTS and MTS treated with GlcN were paralleled by comparatively small reduction in the rate of buildup of FUDP-Hex; this observation indicates a more efficient turnover of FUDP/FUTP into FUDP-Hex in GlcN-treated MTS. Finally, inhibition of *de novo* UMP synthesis by AzaUrd resulted in faster buildup of FUDP-Hex, an unexpected effect which is at variance with the effect of AzaUrd in GlcN-treated MTS in the absence of FUrd; the reason for this effect cannot be deduced from the present NMR data, but it points to the possibility of a specific regulatory role of FUrd.

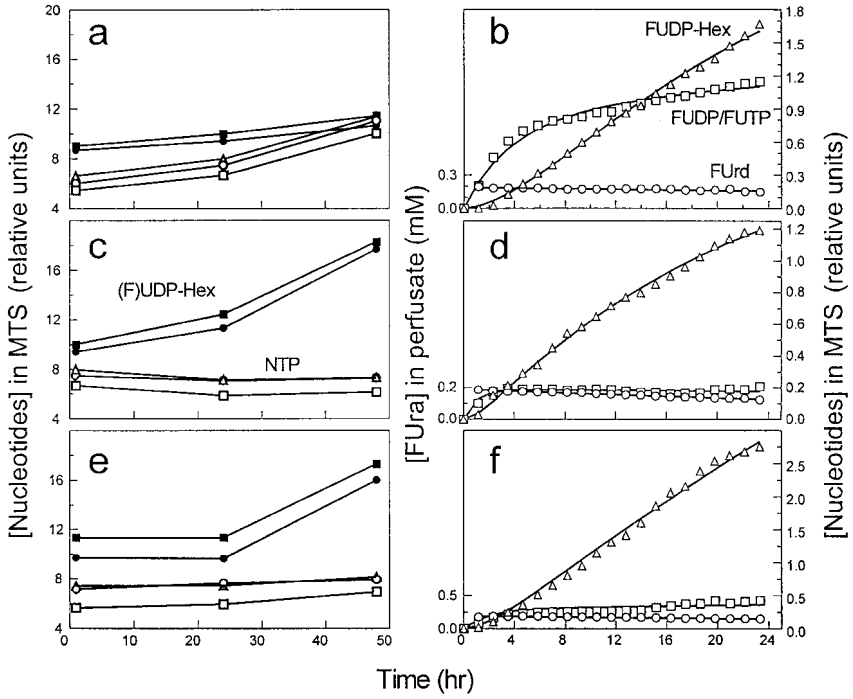

Figure 6. (a), (c) and (e) Time dependence of intracellular levels of (fluoropyrimidine)-phosphates measured by ^{31}P NMR in MTS perfused with serum-free McCoy's medium in the absence (a) and presence of 10 mM GlcN (c, e) measured as in Fig. 2 during the 1st, 24th and 48th hour of experiment. Symbols as in Fig. 2b. Panel (e) represents data obtained from MTS incubated with both GlcN and AzaUrd (0.5 mM). FUrd (initial concentration, 0.19 mM) was added to MTS at the beginning of the 25th hour. (b), (d) and (f). Time dependence of FUrd concentrations in perfusates and of the amounts of metabolites in MTS studied in (a), (c) and (e), respectively, measured by ^{19}F NMR. Note that ordinates in (b), (d) and (f) are not to scale. Other conditions as in Fig. 5

Table 1. Best-fit values for coefficients of model functions [eqs, 1–4] fitted to data in Figs 5 and 6

Treatment	$k_p/10^{-4}$ (/min)	$k_g/10^{-4}$ (/min/M)	$k_r/10^{-4}$ (/min)	$k_f/10^{-4}$ (/min)	χ^2
FUra	10.28 ± 0.07	1.48 ± 0.1	0	20 ± 2	0.0066[a]
FUra + GlcN	4.38 ± 0.06	3.6 ± 0.7	0	21 ± 7	0.0063
FUrd	194 ± 6	1.28 ± 0.05	17 ± 1	6.5 ± 0.8	0.0412
FUrd + GlcN	170 ± 20	2.7 ± 0.1	92 ± 15	5.6 ± 0.9	0.0124
FUrd + GlcN + 6-AzaUrd	134 ± 1	3.1 ± 0.3	0	2 ± 1	0.1566

[a] Low χ^2 values result from an overestimated weighting factor inherent in MLAB software.

Quantitative analysis of FUra and FUrd metabolism by compartmental models

To quantify the effects of GlcN on the kinetics of the observable individual steps in FUra and FUrd metabolism, we analyzed the data in Figs 5b, 5d, 6b, 6d, and 6f by fitting functions of the compartmental model of mass transfer of fluoropyrimidine metabolites described in the Materials and Methods. The best-fit parameter values and the corresponding χ^2-values are shown in Table 1.

The comparison of best-fit values for rate constants in FUra-treated spheroids in the absence and in the presence of GlcN indicated that GlcN reduced the efficiency in FUra uptake and/or fluoropyrimidine phosphate formation (k_p-process; $p < 0.01$) and increased the efficiency of FUDP-Hex formation (k_g-process; $p < 0.01$). However, the metabolism of FUrd in control MTS and in GlcN-treated MTS appeared to be different from the metabolism of FUra. The major differences include the substantive loss of ^{19}F NMR-detectable metabolites in FUrd-treated MTS by the process characterized by the rate constant k_r ($p < 0.01$). In FUrd-treated MTS, GlcN had no effect on k_p ($p = 0.25$), doubled the value of k_g ($p < 0.01$) and quadrupled the value of k_r ($p < 0.01$),

demonstrating the complex effects of GlcN on FUrd metabolism. In MTS treated with FUra, GlcN had no effect on the k_r-process ($k_r = 0$), but in MTS treated with FUrd the effect was substantial ($p < 0.01$).

Introduction of AzaUrd to GlcN-treated MTS had no effect on FUrd uptake and/or fluoropyrimidine phosphate formation (k_p-process). AzaUrd reduced the efficiency of replenishing the F_p-compartment from the F_g-compartment (smaller k_f-values, $p < 0.01$, that were unaffected by GlcN alone, $p = 0.45$) and abolished the disappearance of ^{19}F NMR-detectable metabolites ($k_r = 0$). AzaUrd did not affect the value of k_g ($p = 0.2$). In this comparison of parameters, all statistically significant differences are large compared with standard deviations. Therefore, even allowing for substantial uncertainty in estimates of standard deviations (sometimes inherent in estimating by local Hessian), the significance of differences among parameters remains unchanged.

To provide a basis for comparison of data in Figs 5 and 6 with our earlier data,[10] we fitted model functions in eqs 2–5 to data in Fig. 2 in Chen *et al.*[10] (Table 2). These functions yielded somewhat better fits (lower χ^2-values) than those in Chen *et al.*[10] As expected, the rate-constant values obtained under identical conditions (FUra and FUrd alone) were quite similar between experiments reported in Chen *et al.*[10] and here. On the other hand, the somatostatin analogue octreotide, studied in Chen *et al.*[10] induced modifications of fluoropyrimidine metabolism in a manner different from modifications induced by GlcN. For example, octreotide stimulated the k_r-process in FUra-treated MTS and partially inhibited it in FUrd-treated cells.

DISCUSSION

We used metabolic perturbation in an attempt to define a model of NMR-detectable steps in fluoropyrimidine metabolism. Such a model might help interpret the interactions of FUra and FUrd with metabolic modifiers[2] or with biologic response modifiers such as octreotide, a long-acting somatostatin analogue.[14] We perturbed the metabolism of FUra and FUrd by GlcN because the interactions of this agent with fluoropyrimidines have been characterized rather well[2,14,15] and because GlcN, intriguingly, cured human tumor xenografts in immunodeficient mice when co-administered with FUrd, but not FUra.[15] The specific differences between interactions of GlcN with FUra and FUrd underlying different antitumor effects have not been elucidated.

We hypothesized that some differences in the mechanism of action between GlcN combined with FUra and with FUrd, respectively, could be detected by measuring the kinetics of fluoropyrimidine metabolism or, at least, that kinetic data could generate hypotheses on the mechanisms testable by other methods (e.g. molecular biology). For that, we measured changes in the amounts of total ^{31}P-NMR-detectable phosphates and of ^{19}F-NMR-detectable fluoropyrimidines and evaluated the ^{19}F data by fitting compartmental mathematical models[10] that yielded numerical values for the rate constants characterizing movement of metabolites among the compartments detectable by NMR or known *a priori* (i.e. FUra, FUrd, glucose and GlcN in the medium at the beginning of experiment). In interpreting the current and earlier data, this method has been robust in identifying the best-fit model, and yielded fits comparable with or better than previous models.[10]

Generally, our NMR observations agree with the HPLC results by Keppler and colleagues in studies of HT-29 cells *in vitro*[15] and human breast cancer cells TA3 *in vitro* and grown as xenografts.[16] It is noteworthy that the changes in fluoropyrimidine phosphate concentrations measured by ^{19}F NMR were smooth and in some cases almost linear, indicating continuous metabolic activity under these conditions. In other words, the MTS retained viability throughout these experiments, consistent with the observation that GlcN was cytostatic, but not toxic, for HT-29 cells.[14]

The ^{19}F NMR data were analyzed in detail by the use of mathematical models for qualitative and quantitative differences in the mass transfer of FUra and FUrd metabolites and effects of GlcN. These models allowed an evaluation of the second-order kinetics; for comparison with the present data, we re-evaluated our previously published results on modulation of FUra and FUrd metabolism by the somatostatin analogue octreotide (Chen *et al.*;[10] see below). The best-fit model to each data set was statistically sound and robust and yielded numerical values for the rate constants characterizing each observed mass transfer step. It is noteworthy that the relationship of these empirical constants to the rate constants measured in solutions of isolated components is unclear and that, most likely, is *only formal*. Namely, the empirical constants derived in this work reflect not only the intrinsic kinetic characteristics of a defined catalytic system with a constant enzyme concentration, but are also influenced by the possible changes in enzyme concentrations induced by the 24-h preincubation with GlcN and/or further 24-h (co)incubation with the fluoropyrimidine. Thus, the numerical values of these rate constants are statistically reliable, but they are empirical, relative and mechanistically not necessarily fully understood. Their advantage is that they can quantify the role of each metabolic step within the context of complex changes.

Previously, we observed that k_p, the rate constant for accumulation of FUDP/FUTP, was affected by octreotide differently in HT-29 MTS incubated with FUra than in MTS incubated with FUrd.[10] This phenomenon could be attributed to different mechanisms of FUra and FUrd transport into cells.[2] On the other hand, differences in magnitude of transport-independent processes characterized by k_r and k_f between MTS treated with FUra and

Table 2. Best-fit values for coefficients of model functions [eqs 1–4] fitted to data in Fig. 2 in Chen *et al.*[10]

Treatment	$k_p/10^{-4}$ (/min)	$k_g/10^{-4}$ (/min/M)	$k_r/10^{-4}$ (/min)	$k_f/10^{-4}$ (/min)	χ^2
Fura	16.3 ± 0.7	1.2 ± 0.1	0	15 ± 3	0.0206
FUra + octreotide	12.1 ± 0.5	1.25 ± 0.08	9 ± 1	8 ± 1	0.0053
FUrd	220 ± 4	1.25 ± 0.02	21.3 ± 0.9	4.7 ± 0.5	0.0096
FUrd + octreotide	115 ± 4	1.36 ± 0.07	12 ± 1	9 ± 1	0.0170

[a] Low χ^2 values result from an overestimated weighting factor inherent in MLAB software.

FUrd, in the absence and in the presence of octreotide, were not easily understood. Once FUra had been converted into FUrd, the metabolic pathways of the two drugs are thought to be identical;[2] hence, the observed differences between FUra and FUrd metabolism indicate the effectiveness of a regulatory mechanism dependent either on the initial form of the drug (base vs nucleoside) or on the relative differences in concentrations of metabolites derived from the two forms of the drug or from both.

A scrutiny of the results in Table 1 and the comparison with results in Table 2 reveals consistent patterns in metabolism of FUra and FUrd in MTS, but also specific differences in the metabolism of the two drugs and the regulation by GlcN and octreotide. For example, k_p, the rate constant for the formation of fluoropyrimidine phosphates, was one order of magnitude larger for FUrd than for FUra, but GlcN reduced this rate to half the control in FUra-treated MTS; it had little effect in FUrd-treated MTS. This effect of GlcN, specific for FUra-treated MTS, could result from a decrease in efficiency of FUra uptake, from a reduced formation of FUrd (e.g. by inhibition of uridine phosphorylase), FUMP (inhibition of uridine kinase and/or pyrimidine phosphoribosyl transferase) and FUDP/FUTP, or a combination of these (and other) inhibitory effects. Because FUrd traverses the cell membrane by a mechanism distinct (and more efficient) from the transport of FUra, and because it does not require catalysis by uridine phosphorylase, uridine kinase and pyrimidine phosphoribosyl transferase, the lack of effect of GlcN on the value of k_p in FUrd-treated MTS is compatible with inhibition by GlcN of one or more steps leading from extracellular FUra to FUMP and not with the inhibition of the subsequent formation of FUTP. This notion is corroborated by the apparent lack of product inhibition in generating FUDP/FUTP from FUrd, which indicates that it is unlikely that such inhibition would limit the k_p process in FUra-treated MTS.

While the inhibitory effect of GlcN on k_p was much more pronounced in MTS treated with FUra, the inhibitory effect of octreotide was larger in those treated with FUrd. GlcN strongly stimulated (F)UDP-Hex formation (k_g-process), but octreotide had no effect; in fact, the k_g-values for all experiments conducted in the absence of GlcN were remarkably similar (Tables 1 and 2).

Under our experimental conditions, the escape of metabolites from detection by ^{19}F NMR (by adsorption to and/or incorporation into macromolecules) was not detected in MTS treated with FUra ($k_r = 0$), but was substantial ($k_r > 0$) in MTS treated with FUrd. (Note that we did not detect any loss due to catabolism; cf. Chen *et al.*[10]) The reason for this difference, possibly involving different regulation of RNA polymerase, is unclear. Interestingly, however, GlcN enhanced the k_r-process five-fold in FUrd-treated MTS, but it did not change k_f which measures the efficiency of FUDP-Hex-mediated glycosylation and the return of the resulting FUDP to the FUDP/FUTP pool. Altogether, in FUra-treated MTS, GlcN reduced the generation of FUDP/FUTP and had no effect on the incorporation of FUra into macromolecules. *On the other hand, in FUrd-treated MTS, GlcN did not limit the generation of FUDP/FUTP, but strongly stimulated its incorporation into macromolecules*. It is tempting to speculate that these pharmacokinetic differences underlie the curative effect of GlcN in tumor xenografts treated with FUrd, but not with FUra.[15]

In conclusion, MTS provided a three-dimensional tissue culture model useful for metabolic studies of fluoropyrimidines by NMR. By the use of specifically designed mathematical models we obtained values for the empirical rate constants characterizing mass transfer among the metabolic compartments. An analysis of these rate constants indicated qualitative and quantitative differences in the metabolism of FUra and FUrd and in the effects of GlcN on these drugs. The enhanced generation of FUDP-Hex was a predicted effect of GlcN, but the inhibited FUDP/FUTP formation in FUra-treated MTS and the stimulated fluoropyrimidine incorporation into macromolecules in FUrd-treated MTS were not predicted.

Acknowledgements

We thank Drs Miljenko Huzak and Nenad Juranić for help with NMR experiments and data processing. This work was supported in part by a grant from the Fraternal Order of Eagles.

REFERENCES

1. Heidelberger, C., Chaudhuri, N. K., Danneberg, P., Mooren, D., Griesbach, L., Duschinsky, R., Schnitzer, R. J., Pleven, E. and Scheiner, J. Fluorinated pyrimidines, a new class of tumour-inhibitory compounds. *Nature* **179**, 663–666 (1957).
2. Weckbecker, G. Biochemical pharmacology and analysis of fluoropyrimidines alone and in combination with modulators. *Pharmac. Ther.* **50**, 367–424 (1991).
3. Grem, J. L., Hoth, D. F., Hamilton, J. M., King, S. A. and Leyland-Jones, B. Overview of current status and future direction of clinical trials with 5-fluorouracil in combination with folinic acid. *Cancer Treat. Rep.* **71**, 1249–1264 (1987).
4. Vokes, E. E. Fluorouracil modulation in head and neck cancer. *Adv. Exp. Med. Biol.* **339**, 197–208, (1993).
5. McSheehy, P. M. J. and Griffiths, J. R. ^{19}F MRS studies of fluoropyrimidine chemotherapy. A review. *NMR Biomed.* **2**, 133–141 (1989).
6. Miller, B. E., Miller, F. R. and Heppner, G. H. Assessing tumor drug sensitivity by a new in vitro assay which preserves tumor heterogeneity and subpopulation interactions. *J. Cell Physiol.* **3**, 105–116 (1984).
7. Miller, B. E., Miller, F. R. and Heppner, G. H. Factors affecting growth and drug sensitivity of mouse mammary tumor lines in collagen gel cultures. *Cancer Res.* **45**, 4200–4205 (1985).
8. Pizao, P. E., Lyaruu, D. M., Peters, G. J., van Ark-Otte, J., Winograd, B., Giaccone, G. and Pinedo, H. M. Growth, morphology and chemosensitivity studies on postconfluent cells cultured in 'U'-bottomed microtiter plates. *Br. J. Cancer* **66**, 660–665 (1992).
9. Frankel, A., Buckman, R. and Kerbel, R. S. Abrogation of taxol-induced G_2-M arrest and apoptosis in human ovarian cancer cells grown as multicellular tumor spheroids. *Cancer Res.* **57**, 2388–2393 (1997).
10. Chen, T.-B., Huzak, M., Macura, S. and Vuk-Pavlović, S. Somatostatin analogue octreotide modulates metabolism and effects of 5-fluorouracil and 5-fluorouridine in human colon cancer spheroids. *Cancer Lett.* **86**, 41–51 (1994).
11. Li, S.-J., Wehrle, J. P., Glickson, J. D., Kumar, N. and Braunschweiger, P. G. Tumor bioenergetics and blood flow in RIF-1 murine tumors treated with 5-fluorouracil. *Magn. Reson. Med.* **22**, 47–56 (1991).
12. Kamm, Y. J. L., Rietjens, I. M. C. M., Vervoort, J., Heerschap, A., Rosenbusch, G., Hofs, H. P. and Wagener, D. J. T. Effect of modulators of 5-fluorouracil metabolite patterns in murine colon carcinoma determined by *in vitro* ^{19}F nuclear magnetic resonance spectroscopy. *Cancer Res.* **54**, 4321–4326 (1994).
13. Kaplan, O. and Cohen, J. S. Metabolism of breast cancer cells as revealed by non-invasive magnetic resonance spectroscopy studies. *Breast Cancer Res. Treat.* **31**, 285–299 (1994).
14. Krug, E., Zweibaum, A., Schulz-Holstege, C. and Keppler, D. D-Glucosamine-induced changes in nucleotide metabolism and growth of colon carcinoma cells in culture. *Biochem. J.* **217**, 701–708 (1984).
15. Holstege, A. and Keppler, D. Effects of D-glucosamine and 6-azauridine on nucleotide contents, 5-fluorouridine uptake, and cytotoxicity in TA3 mammary tumor cells. *J. Natl Cancer Inst.* **76**, 485–492 (1986).
16. Pederson, N. V., Zanghi, J. A., Miller, W. M. and Knop, R. H. Discrimination of fluorinated uridine metabolites in N-417 small cell lung cancer cell extracts via ^{19}F- and ^{31}P-NMR. *Magn. Reson. Med.* **31**, 224–228 (1994).
17. Chouini-Lalanne, N., Malet-Martino, M. C., Martino, R. and Michel, G. Study of the metabolism of flucytosine in *Aspergillus* species by ^{19}F nuclear magnetic resonance spectroscopy. *Antimicrob. Agents Chemother.* **33**, 1939–1945 (1989).
18. Pederson, N. V., Knop, R. H. and Miller, W. M. UDP-N-acetylhexosamine modulation by glucosamine and uridine in NCI N-417 variant small cell lung cancer cells: ^{31}P nuclear magnetic resonance results. *Cancer Res.* **52**, 3782–3786 (1992).
19. Bunow, B. and Knott, G. MLAB Reference Manual, Bethesda, MD, Civilized Software (1993).
20. Cook, R. D. and Weinberg, S., Linear and nonlinear regression. In Statistical Methodology in the Pharmaceutical Sciences (Berry, D. A., ed.), p. 163, Marcel Dekker, New York (1990).
21. Crow, E. L., Davis, F. A. and Maxfield, M. W. Statistics Manual, p. 53, Dover, New York (1960).
22. Sheed, S. F., Lutz, N. W. and Hull, W. E. The influence of medium formulation on phosphomonester and UDP-hexose levels in cultured human colon tumor cells as observed by ^{31}P NMR spectroscopy. *NMR Biomed.* **6**, 254–263 (1993).